THE JOURNAL OF PHYSICAL CHEMISTRY C

pubs.acs.org/JPCC

Article

Electronic Excitations in Copper Oxides: Time-Dependent Density Functional Theory Calculations with a Self-Consistent Hybrid Kernel

Aleksandar Živković,* Nora H. de Leeuw, Barry G. Searle, and Leonardo Bernasconi*

Cite This: https://dx.doi.org/10.1021/acs.jpcc.0c08270

Read Online

ACCESS | Metrics & More | Article Recommendations

ABSTRACT: A theoretical study of the electronic structure and optical response of three copper oxides (Cu_2O, Cu_4O_3, and CuO) in the crystalline state is performed using an all-electron perturbative method based on time-dependent density functional theory. We use hybrid density functional theory to account reliably for the direct and indirect semiconducting nature of these materials, as well as for their magnetic ground state. We consider both global and range-separated standard functionals with empirical Hartree−Fock exchange fractions (B3LYP and HSE06) and functionals in which the fraction of Hartree−Fock exchange is determined from a self-consistent procedure, which requires the calculation of the static dielectric constant in the linear-response approximation. Hybrid exchange is found to be essential to reproduce the experimentally observed optical response of the three oxides. The excited-state calculations yield excellent agreement with experiment for the first optically allowed electronic transitions (with excitonic character) of Cu_2O. For Cu_4O_3, an exciton with a small binding energy can be associated with experimentally observed optical features. In CuO, only one dipole allowed transition is found to contribute to the low-energy region of the optical spectrum.

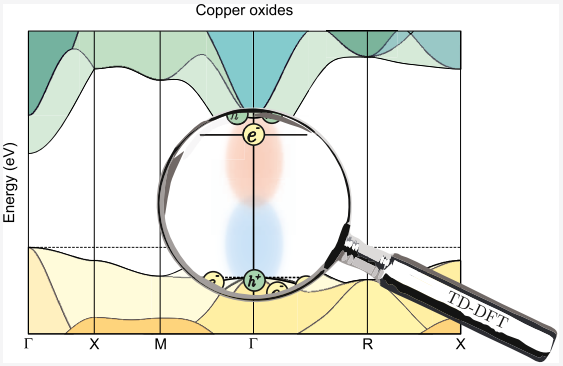

1. INTRODUCTION

The electronic and optical properties of copper oxides have been studied extensively since the early 20th century, owing to their potential applicability in fields including high-temperature superconductivity,[1] water splitting,[2] and gas sensing.[3] Gross et al.[4] in 1956 were amongst the first to relate the narrow lines observed in a spectrogram to exciton formation in the Cu_2O lattice. The yellow and green series of excitations in Cu_2O crystals were measured and characterized as "free" excitations (or Wannier−Mott excitons). Based on these findings, Elliot[5] used band theory to verify the (electric dipole) parity-forbidden nature of the transition between the states immediately above and below the Fermi energy. The valence band was also predicted to split owing to spin-orbit coupling, to give rise to yellow and green exciton series. Fröhlich et al.[6,7] recorded for the first time a detailed two-photon spectrum, which gave evidence for a strong yellow-green exciton mixing and made it possible to observe even-parity excitons directly. Because of its extraordinarily long exciton lifetimes, Cu_2O has been proposed as a potential candidate for the observation of Bose−Einstein condensation of excitons.[8] Evidence has also been put forward for the polaritonic nature of these exciton states.[9] Fishman et al.[10] studied the magneto-optical properties of the yellow exciton series of Cu_2O. Due to the symmetry breaking caused by a magnetic field, the direct emission by the normally optically inactive (dark) para-exciton state was observed successfully. Furthermore, Malerba et al.[11] highlighted the importance of indirect (phonon-assisted) transitions within the green exciton series. Various computational techniques, ranging from tight binding,[12] self-consistent OLCAO + LDA,[13] G_0W_0, and scGW[14] to Hamiltonian modeling[15] were used to study excitons in Cu_2O.

A renewed wave of interest in the Cu_2O exciton spectrum was sparked in 2014, after Kazimierczuk et al.[16] observed large highly excited exciton states in the crystal. These so-called giant Rydberg excitons were observed in Cu_2O with a principal quantum number as large as $n = 25$ and a wave function extending over more than 2 μm (compared to ca. 1 nanometer for the ground-state one), a solid-state analogue of a Rydberg atom.[17] Omelchenko et al.[18] demonstrated the fundamental role of excitons in the photovoltaic properties of Cu_2O, which showed that the so-called "free carrier" model, where electrons and holes behave as independent particles, fails to account for the photoconversion as well as the charge-transport mechanisms. In a Cu_2O photovoltaic cell operating at 300 K, up to 28% of the photogenerated carriers were identified as excitons,

Received: September 10, 2020
Revised: October 16, 2020

while at lower temperatures, excitons were found to be the dominant contributors to the charge-carrier population.

The excitation spectrum of cupric oxide (CuO) has received comparatively less attention. The strong interplay of magnetism, electron−phonon interactions, and charge-transfer features near the absorption edge complicates the interpretation of the optical response of this material. Sukhorukov et al.[21] presented one of the first measurements of the optical absorption profile of CuO single crystals in the range of 80−300 K. The existence of a charge-transfer excitation was proposed involving the Cu 3d−O 2p hybrid ground state and crystal states with pure O character. Two bands at 1.7 and 2.3 eV were assigned to excitonic states, because of their small sensitivity to temperature. Ito et al.[22] determined the complex dielectric function of both Cu_2O and CuO and observed a lack of sharp (exciton) structures in the spectrum of CuO, which was explained in terms of the lower symmetry of the CuO crystal. However, by means of a numerical fit, distinct features at $E_1 \sim 1.6$ eV, $E_2 \sim 2.0$ eV, $E_3 \sim 2.6$ eV, and $E_4 \sim 3.4$ eV were observed, with only E_1 being speculated to correspond to a band-to-band transition at the Γ-point. Masumi et al.[23] reported optical absorption measurements of CuO at various temperatures between 7 and 300 K. Two peaks were observed at $E_A = 1.57511$ eV and $E_B = 1.58097$ eV, but the transitions could not be interpreted in terms of either direct allowed excitations or transitions between magnetically ordered localized states with exchange interaction (charge-transfer type). Sukhorukov et al.[24] also put forward evidence for the existence of a parity allowed indirect transition across the band gap.

Wu et al.[25] investigated d−d excitations in CuO using nonresonant inelastic X-ray scattering. A clear 1.8 eV feature was assigned to the on-site $d_{x^2-y^2} \rightarrow d_{xy}$ transition, while two other transitions, occurring at 2.1 and 2.2 eV, were attributed to $d_{x^2-y^2} \rightarrow d_{yz/zx}$ and $d_{x^2-y^2} \rightarrow d_{3z^2-r^2}$ transitions, respectively. This study supported previous wave-function-based electronic structure calculations, which indicated the existence of transitions from occupied $d_{x^2-y^2}$ orbitals to virtual d_{xy}, d_z^2, d_{xz}, and d_{yz} orbitals.[26] Huotari et al.[27] studied the d−d excitation spectrum of bulk CuO as a function of temperature, and correlated the temperature-dependent 3d band broadening to electron−ion interactions and orbital mixing.

Early calculations of the electronic response of CuO date back to the work of Takahashi et al.,[28] who used a three-body scattering approximation on a multi-orbital tight-binding model to compute absorption spectra in good agreement with experiment. Rödl et al.[29,30] performed nonresonant inelastic X-ray scattering experiments and Green's function calculations (self-consistent GW and Bethe−Salpeter equation, GW-BSE). The lowest optical excitations of CuO were confirmed to correspond to transitions from highest valence states with mixed Cu $3d_{x^2-y^2}$ and O 2p character to empty Cu $3d_{x^2-y^2}$ orbitals, followed by a transition from O 2p states to Cu $3d_{x^2-y^2}$ states. A conservation of the local electronic structure was observed in the paramagnetic phase of CuO, as no strong temperature dependence of the spectral features was observed.

Cu_4O_3 remains the least examined copper oxide, owing to its scarcity and long-debated stability. A comprehensive examination of the electronic properties and absorption features of Cu_4O_3 (along with Cu_2O and CuO), using photoemission spectroscopy, optical absorption coefficient measurements, electron energy loss spectroscopy (ELNES), and many-body perturbation theory calculations (in the form of GW) was presented by Wang et al.[31] Their combined experimental and theoretical approach obtained a consistent picture where the Cu d photoemission peaks of Cu^{2+} and Cu^{1+} lie around −4 and −3 eV relative to the valence band maximum, respectively, across all three examined oxides of copper. The O 2p states were observed to stretch over the entire valence band energy range. It was also found that the interpretation of photoemission data for CuO and Cu_4O_3 is subject to surface reduction under vacuum conditions, making the peak positions hardly distinguishable. The many-body GW calculations (employing an additional onsite potential for the Cu d orbital energies) were able to predict an indirect band gap of 0.84 eV and a direct band gap of 1.59 eV, whereas the experimental optical absorption threshold energy was measured at 1.37 eV.

In this paper, we examine the electronic structure of the three copper oxides using hybrid density functional theory (DFT) and time-dependent density functional theory (TD-DFT) with a fully periodic description of the crystal structure of these materials.[32,33] TD-DFT is currently one of the most advanced and versatile approaches to the calculation of the excited-state properties of finite and extended systems. In a number of situations, its accuracy in crystals can be considered comparable to high-level Green's function theory approaches (GW-BSE), but with a significantly reduced computational cost, provided sufficiently advanced approximations for the ground-state electronic structure in DFT and for the description of its response to electromagnetic perturbations are employed. In particular, the accurate description of bound excitons in TD-DFT has been the subject of considerable work, using a variety of techniques, from semiempirical response kernels, to fully self-consistent approaches.[34−40] More recently, TD-DFT with dielectrically screened hybrid functionals has been demonstrated to be a very promising alternative to the Bethe−Salpeter equation.[41,42]

Here, we extend the TD-DFT approach presented in refs 43, 44, which has been shown to give excellent agreement between calculated and experimental optical transition energies for, among others, simple semiconductors and oxides[43] and chalcopyrite materials[45] for photovoltaic applications (including accurate estimates of exciton energies and binding energies), provided hybrid prescriptions like B3LYP are used both for the DFT exchange−correlation functional and for the nonlocal TD-DFT response kernel. The case of wide-gap insulators, like LiF,[46] appears to be more problematic for functionals like B3LYP, and a semiempirical adjustment of the fraction of exact exchange was found to be necessary to obtain an accurate estimate of the optical gap. In this work, we apply the same approach to the calculation of the optical response of the copper oxides, using a modified B3LYP-like functional in which the exact exchange fraction is determined *ab initio* using the iterative procedure of refs 47, 48.

This paper is organized as follows. In Section 2, we give details of the computational procedure used in the calculations. The results concerning the DFT band structures and TD-DFT response profiles are presented in Section 3. Our conclusions are summarized in Section 4.

2. COMPUTATIONAL DETAILS

DFT calculations presented in this work were performed using the all-electron code CRYSTAL[32,33] (a locally modified version of CRYSTAL14), with a triple-ζ-valence + polarization Gaussian-type basis set optimized for copper oxides by Linnera et al.[49,50] The hybrid B3LYP exchange−correlation func-

https://dx.doi.org/10.1021/acs.jpcc.0c08270
J. Phys. Chem. C XXXX, XXX, XXX−XXX

tional[51,52] was used in all calculations. The fraction of exact Hartree−Fock exchange in the B3LYP functional was modified as indicated below. For all three oxide crystals, the convergence of the total energy with respect to the k-point sampling of the Brillouin zone was assessed. Monkhorst−Pack meshes[53] of 9 × 9 × 9 for Cu_2O, 8 × 8 × 8 for Cu_4O_3, and 6 × 8 × 6 for CuO were used.[32] Cu_2O was modeled in a simple cubic nonmagnetic cubic cell, while for Cu_4O_3 and CuO, an antiferromagnetically ordered unit cell, capturing the experimentally observed magnetic propagation vectors,[54−58] was utilized. To avoid errors when comparing DFT results of certain copper oxides with experimentally available results,[59] the experimental crystal structures, lattice constants, and atomic positions for all three materials were adopted throughout the computation.

The optically allowed electronic transitions for the three oxides were estimated by solving time-dependent density functional theory (TD-DFT) equations[34,60,61] in the linear-response approximation at the B3LYP level of theory for the exchange−correlation functional and response kernel. The many-body electronic transitions in a periodic crystal can be computed by solving the generalized eigenvalue equation[62,63]

$$\begin{pmatrix} \mathbf{A} & \mathbf{B} \\ \mathbf{B}^* & \mathbf{A}^* \end{pmatrix} \begin{pmatrix} \mathbf{X}_I \\ \mathbf{Y}_I \end{pmatrix} = \omega_I \begin{pmatrix} -\mathbf{1} & \mathbf{0} \\ \mathbf{0} & \mathbf{1} \end{pmatrix} \begin{pmatrix} \mathbf{X}_I \\ \mathbf{Y}_I \end{pmatrix} \tag{1}$$

where ω_I is interpreted as a transition energy from the ground state to the electronically excited state I and the eigenvectors $\mathbf{X}_I$ and $\mathbf{Y}_I$ determine the probability of transition. In the case of hybrid TD-DFT, the elements of the matrices **A** and **B** are given by

$$A_{ai,bj}^{\mathbf{k}_a\mathbf{k}_i\mathbf{k}_b\mathbf{k}_j} = \delta_{ij}\delta_{ab}\delta_{\mathbf{k}_i\mathbf{k}_j}\delta_{\mathbf{k}_a\mathbf{k}_b}(\varepsilon_a^{\mathbf{k}_a} - \varepsilon_i^{\mathbf{k}_i}) + (a\mathbf{k}_a i\mathbf{k}_i|j\mathbf{k}_j b\mathbf{k}_b) - (a\mathbf{k}_a b\mathbf{k}_b|j\mathbf{k}_j i\mathbf{k}_i)c_{HF} + (a\mathbf{k}_a i\mathbf{k}_i|f_{xc}|j\mathbf{k}_j b\mathbf{k}_b)(1 - c_{HF}) \tag{2}$$

$$B_{ai,bj}^{\mathbf{k}_a\mathbf{k}_i\mathbf{k}_b\mathbf{k}_j} = (a\mathbf{k}_a i\mathbf{k}_i|b\mathbf{k}_b j\mathbf{k}_j) - (a\mathbf{k}_a j\mathbf{k}_j|b\mathbf{k}_b i\mathbf{k}_i)c_{HF} + (a\mathbf{k}_a i\mathbf{k}_i|f_{xc}|b\mathbf{k}_b j\mathbf{k}_j)(1 - c_{HF}) \tag{3}$$

in which the standard quantum-chemical notation for the two-electron integrals is used, and $|l\mathbf{k}_l\rangle$ represents the crystal orbital l at **k**-point k_l of the Brillouin zone. (*i*, *j*) and (*a*, *b*) label occupied and virtual Kohn−Sham orbitals, respectively. f_{xc} is the exchange−correlation kernel of TD-DFT, which we assume here to be in its adiabatic approximation.[64] c_{HF} is the fraction of Hartree−Fock exchange of the hybrid functional used to compute the unperturbed Kohn−Sham orbitals $|l\mathbf{k}_l\rangle$. The solution of eq 1 by either direct or iterative diagonalization is prohibitive for most realistic three-dimensional systems, owing to the dependence of the two-electron Coulomb and exchange response integrals on four band indices and two quasi-momentum indices, which leads to a highly unfavorable scaling with the system size (number of electronic bands) and the number of **k**-points used in the Brillouin zone integration. In the approach described in ref 43, the direct calculation of the **A** and **B** matrix elements is avoided and the eigenvalue problem of eq 1 is replaced by an equivalent self-consistent procedure in the presence of an external perturbation. The perturbed self-consistent Kohn−Sham equations are solved using a periodic generalization of the coupled-perturbed Hartree−Fock/Kohn−Sham method,[65] and transition energies of optically allowed excitations are computed from the poles of the many-body dynamical polarizability tensor $\alpha(\hbar\omega)$ over a given frequency range ω. The lowest-energy pole corresponds to the experimental optical gap of the system under study. However, the study of dipole forbidden excitons (e.g., the yellow/green series of Cu_2O) remains, at least for the time being, outside of what is achievable within this framework. This approach has been shown to provide reliable estimates of (weakly bound) exciton absorption and binding energies in wide classes of semiconductors and insulators[43−45] when c_{HF} is set to a value corresponding to the (empirical) admixture of Hartree−Fock exchange used in standard DFT functionals (e.g., 0.2 for B3LYP). However, large errors (ca. 1 eV in excitation energies) are observed in the case of tightly bound (Frenkel) and charge-transfer excitons, as for example in crystalline LiF.[46] According to the zone-center two-band argument of ref 46, the origin of this error has to be found in the inability of standard hybrid functionals to account quantitatively for the long-range electron−hole Coulomb attraction in terms of a single distance-independent parameter c_{HF} (cf. the discussion of eq 17 in ref 46). A simple tuning c_{HF} can be used to recover the experimental value of the optical gap from hybrid TD-DFT calculations, at the cost, however, of including at least one purely empirical parameter in the calculations.

Skone et al.[47] have proposed a procedure for computing from first principles the constant c_{HF} for any nonmetallic condensed system. As the Coulomb interaction is proportional to the inverse of the static dielectric constant (ϵ_∞^{-1}), they suggested that the parameter c_{HF} can be estimated, for a given material, in terms of this quantity. This assumption can be rigorously justified using many-body perturbation theory.[66] ϵ_∞^{-1} can be determined from first-order perturbation theory by solving a set of coupled-perturbed Kohn−Sham (CP-KS) equations.[65] This approach, applied to semiconducting and insulating materials with standard global hybrid functionals like PBE0[67,68] yields band gaps and dielectric constants that are in general improved compared to other hybrid and nonhybrid functionals, and achieves an accuracy comparable to self-consistent GW procedures.[47] We have applied this procedure to the case of Cu_4O_3 and CuO, which leads to optimal values of $c_{HF}(Cu_4O_3)$ = 0.174 and c_{HF}(CuO) = 0.127, whereas the default value (c_{HF} = 0.20) was used for Cu_2O. The accompanying electronic dielectric function reads values of ϵ = 5.7, 5.8, and 7.8 for Cu_2O, Cu_4O_3, and CuO, respectively. In this work, we apply an analogous method in the context of hybrid TD-DFT calculations. We compute a static dielectric function $\epsilon_\infty^{\text{CP-KS}}$ from the solution of a set of CP-KS equations at the B3LYP level of theory, and we then set the Hartree−Fock exchange fraction in the exchange−correlation functional and eqs 2 and 3, to $c_{HF} = (\epsilon_\infty^{\text{CP-HF}})^{-1}$. Equation 1 is then solved using the approach of ref 43.

3. RESULTS AND DISCUSSION

3.1. Ground-State Properties. Cu_2O is a p-type semiconductor with cubic structure (space group $Pn\bar{3}m$, no. 224).[69] The unit cell contains six atoms, four Cu atoms, which form a face-centered sublattice, and two O atoms, in a body-centered sublattice. The copper atoms are situated at the vertices of a tetrahedron around each oxygen atom. The experimental lattice constant is 4.2696 Å, and the Cu−O bond length is 1.85 Å.[70]

https://dx.doi.org/10.1021/acs.jpcc.0c08270
J. Phys. Chem. C XXXX, XXX, XXX−XXX

CuO adopts a lower symmetry monoclinic structure (space group $C2/c$, no. 15). The unit cell consists of eight atoms, four Cu atoms, and four O atoms. Each copper atom is coordinated by four oxygen atoms in an approximately square planar configuration, while each oxygen atom is located at the center of a Cu distorted tetrahedron,[77] with the following lattice parameters: a = 4.6837 Å, b = 3.4226 Å, c = 5.1288 Å.[13] CuO is one of the few magnetic copper oxides that does not contain other magnetic atoms. Neutron scattering measurements have shown that CuO has antiferromagnetic ordering below (225 ± 5) K (Néel temperature), with an intrinsic magnetic moment of (0.68 ± 0.1) μ_B (values obtained at 78 K) localized entirely on the Cu atoms.[78] The observed doubling of the lattice periodicity along the $\vec{a}$ and $\vec{c}$ axes has been shown to appear in consequence to the antiferromagnetic ordering of the Cu moments. The Cu−O−Cu chains are completely antiferromagnetically arranged along the [010] crystallographic direction (Table 1).

Table 1. Optical Properties of Cu_2O from Literature Results

series name	excitation onset (eV)	excitation limit (eV)
yellow	2.0332 (4.2 K)[4]	2.1719 (4.2 K)[4]
	2.0330 (20 K)[7]	
green	2.131 (4.2 K)[4]	2.303 (4.2 K)[4]
blue	2.531 (77 K)[19]	2.583 (77 K),[19] 2.65 (1.3 K)[8]
	2.583 (6 K)[20]	2.634 (6 K)[20]
violet/indigo	2.637 (77 K)[19]	2.712 (77 K),[19] 2.78 (1.3 K)[8]

Cu_4O_3 (paramelaconite) is found in a tetragonal structure (space group $I4_1/amd$, no. 141), with lattice parameters $a = b$ = 5.837 Å, c = 9.932 Å.[79] The chemical formula of paramelaconite is Cu_2^{1+} Cu_2^{2+} O_3, with two distinct Cu atoms, Cu(1) and Cu(2). Cu(1) has oxidation state +1 and has two nearest-neighbor oxygen atoms, O(1), forming collinear bonds of length 1.87 Å, similar to Cu_2O. Cu(2) has oxidation state +2 and is surrounded by four O atoms in an almost square planar configuration with bond lengths varying between 1.92 and 1.97 Å. Like CuO, Cu_4O_3 orders antiferromagnetically below 40 K with a propagation vector $\vec{k}$ = ((1/2), (1/2), (1/2)) with respect to the reciprocal basis of the conventional body-centered cell.[54]

The calculated single-particle Kohn−Sham electronic band gap values are reported in Table 2, with the corresponding band structures shown in Figure 1. Cu_2O, a band insulator with almost fully occupied Cu 3d states, is found to possess a direct electronic band gap of 2.149 eV at the Γ-point (B3LYP values), in good agreement with the experimentally observed gap of 2.17 eV. The top of the valence band comprises mostly Cu 3d states with non-negligible mixing with O 2p states, while the conduction band arises predominantly from Cu 3d states (Figure 2). These results are in agreement with previously observed trends in Cu_2O.[80]

Tuning the exact exchange value for Cu_2O using the self-consistent dielectric-dependent procedure within the B3LYP approximation (SC-B3LYP) results in a calculated value of 1.916 eV, which is more than 10% lower than the experimentally measured one. For comparison, the band gap calculated using a range-separated hybrid functional (HSE06) with the default exact exchange parameter is close to the SC-B3LYP one. We therefore conclude that, in the case of Cu_2O, the exact exchange tuning procedure does not improve the accuracy of standard B3LYP calculations.

Calculations at the B3LYP level for the electronic structure of Cu_4O_3 yield an indirect fundamental transition between the top valence and the bottom conduction bands of 2.103 eV, while the direct transition at the Γ-point corresponds to 2.526 eV. These values overestimate the experimentally observed lowest indirect transition of 1.3−1.5 eV. Using SC-B3LYP lowers the conduction band edge, and the final indirect and direct band gaps are 1.773 and 2.220 eV, respectively (Figure 1). The orbital-decomposed contribution of the Cu and O atoms to the total density of state for Cu_4O_3 is shown in Figure 3. The top of the valence band, up to −1 eV below on an energetic scale, consists mostly of Cu(1) 3d states strongly mixed with O(1) 2p and, to a lesser extent, with O(2) 2p states. The Cu(2) 3d orbitals, giving rise to the material's magnetic features, are located between −3 and −5 eV below the Fermi level. The conduction band originates predominantly from Cu(2) atoms, in particular $3d_{yz}$ empty orbitals with a slight mixture of O(1) p_x and O(2) p states. These results are in good agreement with X-ray photoemission spectroscopy (XPS), ultraviolet photoemission spectroscopy (UPS), and electron energy loss spectroscopy (ELNES) measurements, as well as with GW calculations.[31] A magnetic moment localized entirely on the Cu(2) atom with a value of 0.595 μ_B, was obtained from the Mulliken spin population analysis, and agrees well with the measured values of 0.46−0.66 μ_B.[81] No net magnetization was observed on the other atoms.

The obtained electronic band structure of CuO is shown in Figure 1. Similar to the other two oxides, B3LYP calculations yield a correct description of the band gap nature (indirect), but the calculated value overestimates the experimentally observed low-temperature band gap of 1.2 eV−1.5 eV. The SC-B3LYP scheme improves these results, and yields an indirect fundamental transition of 1.805 eV between the Γ and M points of the Brillouin zone. Both the valence and conduction bands of CuO originate from strongly mixed Cu 3d and O 2p states (Figure 4), consistent with the model of a strongly correlated Mott/charge-transfer insulator. The calculated magnetic moments of CuO are 0.608 μ_B on Cu^{2+} atoms

Table 2. Kohn−Sham Gaps Obtained from Hybrid DFT Calculations and Experimental Electronic (Transport) Band Gaps[a]

E_g (eV)	c_{HF}	Cu_2O	Cu_4O_3	CuO
B3LYP	0.20	2.149 (d)	2.103 (i)	2.130 (i)
SC-B3LYP	0.168/0.174/0.127	1.916 (d)	1.773 (i)	1.805 (i)
HSE06	0.25	1.926 (d)	2.189 (i)	3.087 (i)
exp.		2.17 (d)[4]	1.34−1.5 (i)[71,72]	1.0−1.9 (i)[24,73,74]
			1.75−2.47 (d)[71,75]	3.25 (d)[76]

[a] c_{HF} denotes the fraction of Hartree−Fock exchange used in DFT calculations using the self-consistent procedure described in the text, while (d) and (i) indicate the direct and indirect natures of the band gap, respectively.

https://dx.doi.org/10.1021/acs.jpcc.0c08270
J. Phys. Chem. C XXXX, XXX, XXX−XXX

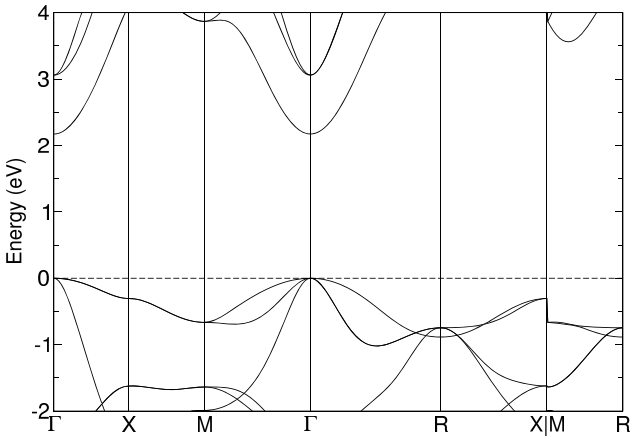

(a) Cu_2O

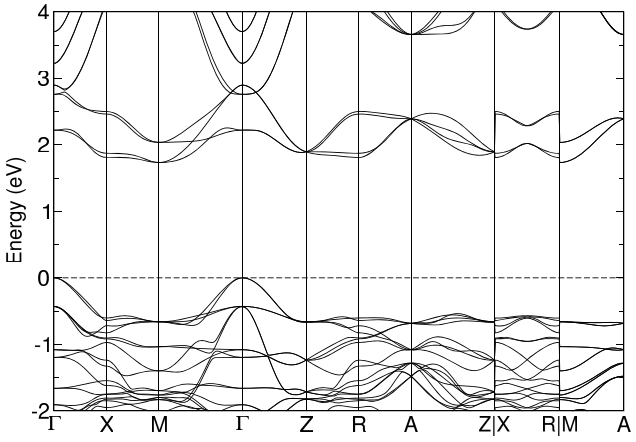

(b) Cu_4O_3

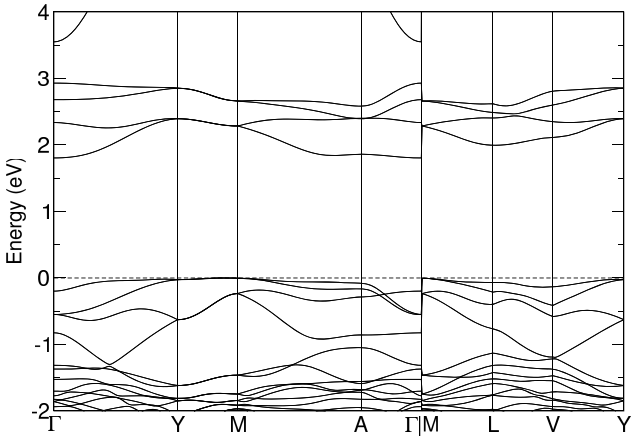

(c) CuO

Figure 1. Electronic band structures of the copper oxides, obtained using the DFT (SC-)B3LYP approximation. The dashed line indicates the highest occupied valence state.

and 0.183 μ_B on O^{2-} magnetic ions (compared to experimental values of 0.65 and 0.14 μ_B, respectively[82]). Despite the fact that results for the band gap (compared to low-temperature measurements of 1.4−1.5 eV[31,83]) are slightly overestimated, the amount of exact exchange utilized in the calculation was not tuned further to retain the self-consistent nature of determined values and minimize manual adjustments to the system. In addition, results match quantitatively previous CuO data.[25,31]

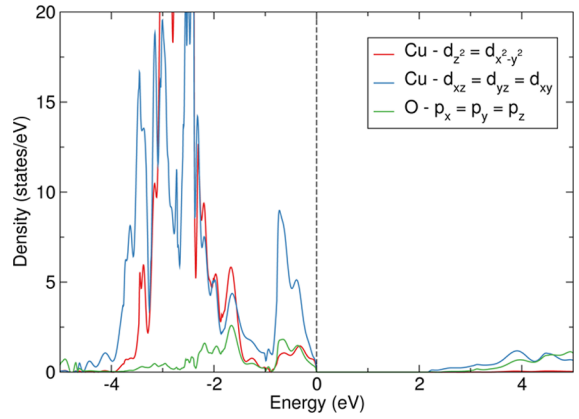

Figure 2. Orbital-decomposed electronic density of Cu d and O p states of Cu_2O obtained using the B3LYP approximation. The dashed line indicates the highest occupied valence state.

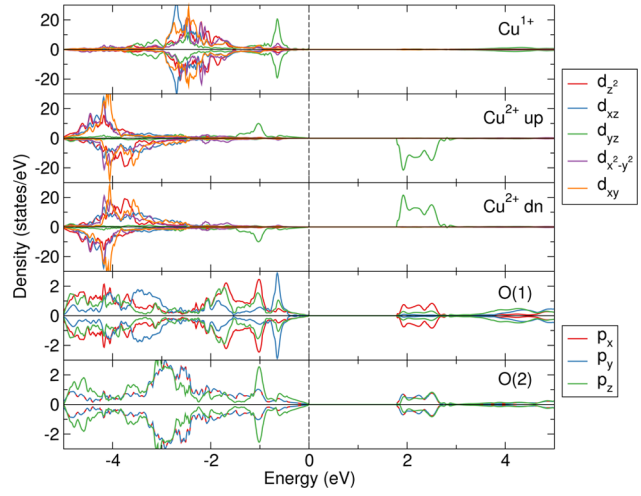

Figure 3. Orbital-decomposed electronic density of Cu d and O p states of Cu_4O_3 obtained using the SC-B3LYP approximation. The dashed line indicates the highest occupied valence state.

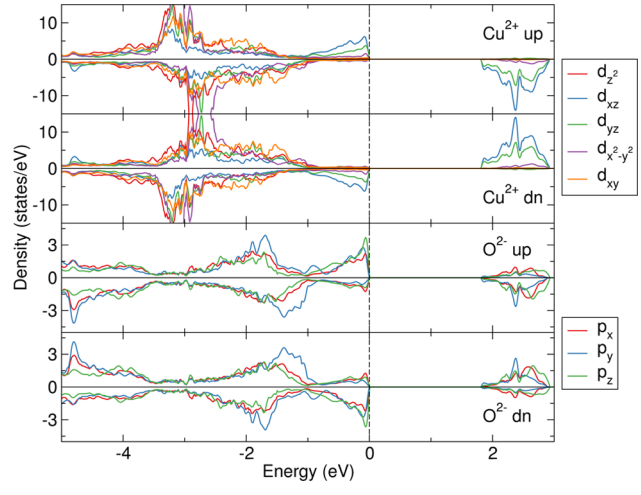

Figure 4. Orbital-decomposed electronic density of Cu d and O p states of CuO obtained using the SC-B3LYP approximation. The dashed line indicates the highest occupied valence state.

3.2. Electronic Excitations. The TD-DFT mean dynamic polarizability (MDP) of the three copper oxides has been

https://dx.doi.org/10.1021/acs.jpcc.0c08270
J. Phys. Chem. C XXXX, XXX, XXX−XXX

estimated using a hybrid B3LYP exchange−correlation kernel (the imaginary part of the dielectric tensor is not readily available at the moment within the outlined approach). The calculated values for Cu_2O are shown in Figure 5 and listed in

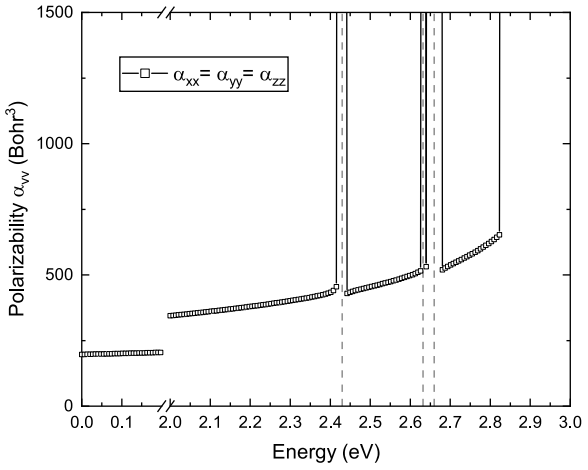

Figure 5. Perturbation energy dependence of the many-body polarizability tensor calculated using TD-B3LYP for Cu_2O. The actual values are presented with white-filled squares, while the black full and gray dashed lines are visual guidelines.

Table 3. Computed Poles of the TD-DFT Mean Dynamic Polarizability of the Three Copper Oxides of Interest, Obtained Using SC-B3LYP

excitation	Cu_2O (eV)	Cu_4O_3 (eV)	CuO (eV)
optically allowed transitions	2.43	2.18	1.93
	2.63	2.28	
	2.66		

Table 3. Since Cu_2O has cubic symmetry, the three crystallographic directions yield the same polarization values (optical isotropy), and therefore only one diagonal component needs to be computed. The first pole of the MDP appears at 2.43 eV, followed by two further absorption peaks at 2.63 and 2.66 eV.

These values are substantially higher than the band gap (2.17 eV), which suggests that they do not correspond to the lowest excitonic transitions observed in Cu_2O, which is the parity-forbidden yellow exciton series mentioned in the Section 1. This is consistent with the fact that our approach only yields optically (dipole-) allowed transitions, but it does not account for quadrupole or dipole magnetic effects, which are responsible for the optical activity of the yellow series. Furthermore, no spin-orbit coupling effects were included in our calculations, and the top $\Gamma_{25'}$ valence band is therefore not split into Γ_8^+ and Γ_7^+ bands. The yellow and green excitonic series would therefore be indistinguishable in our approach, even if higher-order multipole effects were included. Taking this into account, the lowest calculated absorption energy (2.43 eV) can be attributed to the onset of the blue exciton series at 2.531 and the 2.63 eV pole to the violet/indigo excitation onset of 2.637 eV (see Table 1 for complete reference values). Also note that, since we are adopting a purely adiabatic approximation for the nonlocal hybrid kernel, only the fundamental mode of the exciton series can be determined using our approach.[84,85] In conclusion, despite all of the limitations outlined above, TD-DFT with a hybrid B3LYP approximation gives results in excellent agreement with experiment for the blue and indigo excitons of Cu_2O.

In Cu_4O_3, a tetragonal system, two directions are isotropic, and the polarizability is therefore estimated with respect to perturbations along the two nonequivalent directions. The resulting MDP of Cu_4O_3 is shown in Figure 6. The first pole

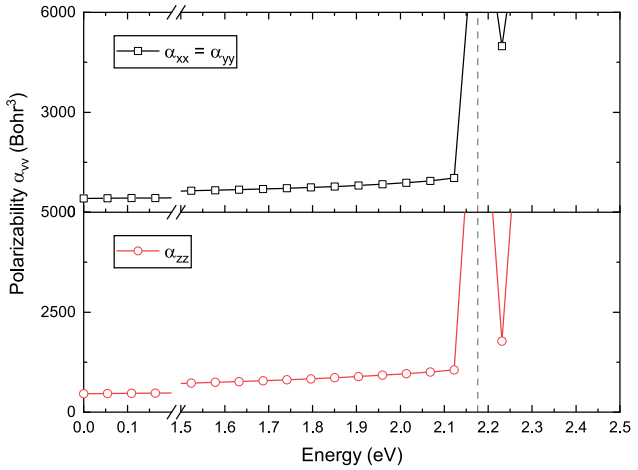

Figure 6. Perturbation energy dependence of the many-body polarizability tensor calculated using TD-B3LYP for Cu_4O_3. The actual values are presented with filled squares and circles, while the full and dashed lines are visual guidelines.

occurs at 2.18 eV, with a following continuum of poles after 2.28 eV arising from band-to-band transitions to conduction states. A further complication of this system, in addition to those of Cu_2O, is the necessary inclusion of electron−phonon coupling in the case of indirect fundamental transitions. The lowest indirect transition between the Γ and the M points cannot therefore be analyzed with our method. The observed pole at 2.18 eV can be attributed to a transition to an exciton state occurring at the Γ-point. The single-particle KS eigenvalues of the first conduction band at the Γ-point is 2.22 eV, which is consistent with a weakly bound (0.04 eV) Wannier−Mott exciton. This transition, according to the computed densities of state, involves empty Cu(2) $3d_{yz}$ orbitals. Furthermore, this transition is dipole allowed, and can be linked to the transitions labeled E2 in the work of Meyer et al.,[86] located at 2.34 eV in spectrometric ellipsometry measurements. The measured peaks show an increased width compared to the sharp lines of Cu_2O, possibly arising from electron−phonon contributions, which could not, however, be unambiguously identified as an exciton transition. Despite the neglect of electron−phonon effect in our calculations, this possible identification is a step forward in the understanding of the absorption processes in Cu_4O_3 crystals.

The third oxide, CuO, is a highly anisotropic crystal, which requires the calculation of the full polarizability tensor. The simulated MDP along the three crystallographic directions is shown in Figure 7. The first and only observed absorption peak is found at 1.93 eV in all three crystallographic directions, after which a continuum of absorption peaks is observed arising from the overlap of continuous conduction states. This pole can be linked to an optically allowed transition at either the Γ or A points, whose single-particle energies are 2.007 and 1.938

https://dx.doi.org/10.1021/acs.jpcc.0c08270
J. Phys. Chem. C XXXX, XXX, XXX−XXX

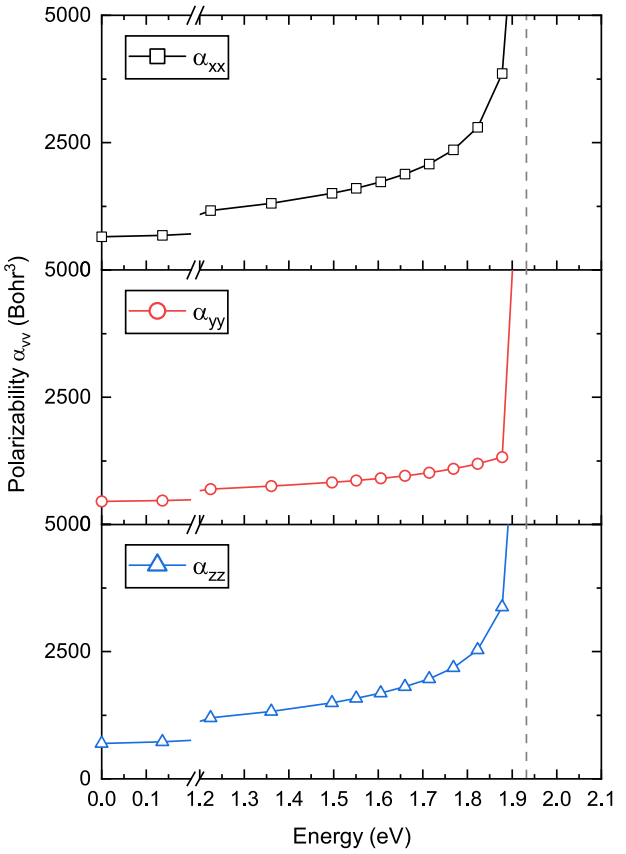

Figure 7. Perturbation energy dependence of the many-body polarizability tensor calculated using TD-B3LYP for CuO. The actual values are presented with filled squares, circles, and triangles, while the full and dashed lines are visual guidelines.

eV, respectively. This transition is likely to originate from a weakly bound (0.01−0.06 eV) extended excitonic state. Taking into account that the calculated value of the KS band gap is ca. 0.4 eV above the experimentally observed low-temperature value and applying this shift to the calculated first MDP pole, a value of ≈ 1.55 eV is obtained. A possible excitation at 1.6 eV was measured by Ito et al.,[87] and one at 1.66 eV by Meyer et al.[86] Since optically allowed transitions result in more intense absorption features, the identified pole is likely to correspond to the experimentally observed peak.

4. CONCLUSIONS

A calculation of electronic and optical properties of three copper oxides (Cu_2O, CuO, and Cu_4O_3) has been performed using DFT and linear-response TD-DFT at a hybrid level of theory (B3LYP), with a variable fraction of exact exchange in the density functional and the exchange−correlation response kernel. The electronic structure of Cu_2O is found to be accurately represented with the default B3LYP fraction of exact exchange, while for Cu_4O_3 and CuO, a self-consistent value shows improved accuracy with respect to experimental data. Optical response calculations account for the blue and violet excitonic series of Cu_2O in excellent agreement with experimental data. A small binding energy exciton has been identified in the case of Cu_4O_3 and linked to existing experimental measurements. For CuO, only one possible excitation peak is calculated.

AUTHOR INFORMATION

Corresponding Authors

Aleksandar Živković − *Department of Earth Sciences, Utrecht University, 3548CB Utrecht, The Netherlands;* orcid.org/0000-0003-1347-6203; Email: a.zivkovic@uu.nl

Leonardo Bernasconi − *Center for Research Computing, University of Pittsburgh, Pittsburgh, Pennsylvania 15260, United States*; Email: leonardo.bernasconi@pitt.edu

Authors

Nora H. de Leeuw − *Department of Earth Sciences, Utrecht University, 3548CB Utrecht, The Netherlands*

Barry G. Searle − *STFC Daresbury Laboratory, WA4 4AD Cheshire, United Kingdom*

Complete contact information is available at: https://pubs.acs.org/10.1021/acs.jpcc.0c08270

Notes

The authors declare no competing financial interest.

ACKNOWLEDGMENTS

Computing resources were provided by STFC Rutherford-Appleton Laboratory. This research was supported in part by the University of Pittsburgh Center for Research Computing through the resources provided.

REFERENCES

(1) Zheng, X. G.; Xu, C. N.; Tomokiyo, Y.; Tanaka, E.; Yamada, H.; Soejima, Y. Observation of Charge Stripes in Cupric Oxide. *Phys. Rev. Lett.* **2000**, *85*, 5170−5173.

(2) Li, L.; Zhang, R.; Vinson, J.; Shirley, E. L.; Greeley, J. P.; Guest, J. R.; Chan, M. K. Y. Imaging Catalytic Activation of CO_2 on Cu_2O (110)—A First-Principles Study. *Chem. Mater.* **2018**, 1912.

(3) Gupta, D.; Meher, S. R.; Illyaskutty, N.; Alex, Z. C. Facile synthesis of Cu_2O and CuO nanoparticles and study of their structural, optical and electronic properties. *J. Alloys Compd.* **2018**, *743*, 737−745.

(4) Gross, E. F. Optical Spectrum of Excitons in the Crystal Lattice. In *Il Nuovo Cimento*, Ser. 10; Springer, 1956; Vol. *3*, pp 672−701.

(5) Elliott, R. J. Symmetry of Excitons in Cu_2O. *J. Phys. Rev.* **1961**, *124*, 340−345.

(6) Fröhlich, D.; Kenklies, R.; Helbig, R. Band-Gap Assignment in SnO_2 by Two-Photon Spectroscopy. *Phys. Rev. Lett.* **1978**, *41*, 1750−1751.

(7) Fröhlich, D.; Kenklies, R.; Uihlein, C.; Schwab, C. Assignment of the Even-Parity Excitons in Cu_2O. *Phys. Rev. Lett.* **1979**, *43*, 1260−1263.

(8) Fishman, D. A.; Revcolevschi, A.; van Loosdrecht, P. H. M. Exciton dynamics in cuprous oxide. *Phys. Status Solidi C* **2006**, *3*, 2469−2472.

(9) Fröhlich, D.; Brandt, J.; Sandfort, C.; Bayer, M.; Stolz, H. High resolution spectroscopy of excitons in Cu_2O. *Phys. Status Solidi B* **2006**, *243*, 2367−2374.

(10) Fishman, D.; Faugeras, C.; Potemski, M.; Revcolevschi, A.; Van Loosdrecht, P. H. Magneto-optical readout of dark exciton distribution in cuprous oxide. *Phys. Rev. B: Condens. Matter Mater. Phys.* **2009**, *80*, 3−8.

(11) Malerba, C.; Biccari, F.; Leonor Azanza Ricardo, C.; DaIncau, M.; Scardi, P.; Mittiga, A. Absorption coefficient of bulk and thin film Cu_2O. *Sol. Energy Mater. Sol. Cells* **2011**, *95*, 2848−2854.

(12) Robertson, J. Electronic structure and X-ray near-edge core spectra of Cu_2O. *Phys. Rev. B* **1983**, *28*, 3378−3385.

(13) Ching, W. Y.; Xu, Y. N.; Wong, K. W. Ground-state and optical properties of Cu_2O and CuO crystals. *Phys. Rev. B* **1989**, *40*, 7684−7695.

https://dx.doi.org/10.1021/acs.jpcc.0c08270
J. Phys. Chem. C XXXX, XXX, XXX−XXX

(14) Bruneval, F.; Vast, N.; Reining, L.; Izquierdo, M.; Sirotti, F.; Barrett, N. Exchange and Correlation Effects in Electronic Excitations of Cu_2O. *Phys. Rev. Lett.* **2006**, *97*, No. 267601.
(15) Schweiner, F.; Main, J.; Wunner, G.; Uihlein, C. Even exciton series in Cu_2O. *Phys. Rev. B* **2017**, *95*, No. 195201.
(16) Kazimierczuk, T.; Fröhlich, D.; Scheel, S.; Stolz, H.; Bayer, M. Giant Rydberg excitons in the copper oxide Cu_2O. *Nature* **2014**, *514*, 343−347.
(17) Gallagher, T. F. Rydberg atoms. *Rep. Prog. Phys.* **1988**, *51*, 143−188.
(18) Omelchenko, S. T.; Tolstova, Y.; Atwater, H. A.; Lewis, N. S. Excitonic Effects in Emerging Photovoltaic Materials: A Case Study in Cu_2O. *ACS Energy Lett.* **2017**, *2*, 431−437.
(19) Brahms, S.; Nikitine, S. Intrinsic absorption and reflection of cuprous oxide in the 2.5 to 6.5 eV region. *Solid State Commun.* **1965**, *3*, 209−212.
(20) Takahata, M.; Naka, N. Photoluminescence properties of the entire excitonic series in Cu_2O. *Phys. Rev. B* **2018**, *98*, No. 195205.
(21) Sukhorukov, Y.; Loshkareva, N. N.; Samokhvalov, A. A.; Moskvin, A. S. Absorption spectra of CuO single crystals near the absorption edge and the nature of the optical gap in copper oxides. *J. Exp. Theor. Phys.* **1995**, *81*, 998−1002.
(22) Ito, T.; Yamaguchi, H.; Masumi, T.; Adachi, S. Optical Properties of CuO Studied by Spectroscopic Ellipsometry. *J. Phys. Soc. Jpn.* **1998**, *67*, 3304−3309.
(23) Masumi, T.; Yamaguchi, H.; Ito, T.; Shimoyama, H. New Fine Structures near the Optical Absorption Edge of CuO at Low Temperatures. *J. Phys. Soc. Jpn.* **1998**, *67*, 67−70.
(24) Sukhorukov, Y.; Loshkareva, N.; Moskvin, A.; Arbuzov, V.; Naumov, S. Influence of electron irradiation on the fundamental absorption edge of a copper monoxide CuO single crystal. *Tech. Phys. Lett.* **1998**, *24*, 5−7.
(25) Wu, W. B.; Hiraoka, N.; Huang, D. J.; Huang, S. W.; Tsuei, K. D.; van Veenendaal, M.; van den Brink, J.; Sekio, Y.; Kimura, T. Effective orbital symmetry of CuO: Examination by nonresonant inelastic X-ray scattering. *Phys. Rev. B* **2013**, *88*, No. 205129.
(26) Huang, H.-Y.; Bogdanov, N. A.; Siurakshina, L.; Fulde, P.; van den Brink, J.; Hozoi, L. Ab initio calculation of d - d excitations in quasi-one-dimensional Cu d^9 correlated materials. *Phys. Rev. B* **2011**, *84*, No. 235125.
(27) Huotari, S.; Simonelli, L.; Sahle, C. J.; Sala, M. M.; Verbeni, R.; Monaco, G. Temperature dependence of crystal field excitations in CuO. *J. Phys.: Condens. Matter* **2014**, *26*, No. 165501.
(28) Takahashi, M.; Igarashi, J.-i. Electronic excitations in cupric oxide. *Phys. Rev. B* **1997**, *56*, 12818−12824.
(29) Rödl, C.; Sottile, F.; Reining, L. Quasiparticle excitations in the photoemission spectrum of CuO from first principles: A GW study. *Phys. Rev. B* **2015**, *91*, No. 045102.
(30) Rödl, C.; Ruotsalainen, K. O.; Sottile, F.; Honkanen, A.-P.; Ablett, J. M.; Rueff, J.-P.; Sirotti, F.; Verbeni, R.; Al-Zein, A.; Reining, L.; Huotari, S. Low-energy electronic excitations and band-gap renormalization in CuO. *Phys. Rev. B* **2017**, *95*, No. 195142.
(31) Wang, Y.; Lany, S.; Ghanbaja, J.; Fagot-Revurat, Y.; Chen, Y. P.; Soldera, F.; Horwat, D.; Mücklich, F.; Pierson, J. F. Electronic structures of Cu_2O, Cu_4O_3, and CuO: A joint experimental and theoretical study. *Phys. Rev. B* **2016**, *94*, No. 245418.
(32) Dovesi, R. et al.et al.*CRYSTAL17 User's Manual*; University Torino: Torino, 2017.
(33) Dovesi, R.; Erba, A.; Orlando, R.; Zicovich-Wilson, C. M.; Civalleri, B.; Maschio, L.; Rérat, M.; Casassa, S.; Baima, J.; Salustro, S.; Kirtman, B. Quantum-mechanical condensed matter simulations with CRYSTAL. *Wiley Interdiscip. Rev.: Comput. Mol. Sci.* **2018**, *8*, 1−36.
(34) Onida, G.; Reining, L.; Rubio, A. Electronic excitations: density-functional versus many-body Green's-function approaches. *Rev. Mod. Phys.* **2002**, *74*, 601−659.
(35) Sole, R. D.; Adragna, G.; Olevano, V.; Reining, L. Long-range behavior and frequency dependence of exchange−correlation kernels in solids. *Phys. Rev. B* **2003**, *67*, No. 045207.
(36) Botti, S.; Sottile, F.; Vast, N.; Olevano, V.; Reining, L.; Weissker, H.-C.; Rubio, A.; Onida, G.; Sole, R. D.; Godby, R. W. Long-range contribution to the exchange−correlation kernel of time-dependent density functional theory. *Phys. Rev. B* **2004**, *69*, No. 155112.
(37) Sharma, S.; Dewhurst, J. K.; Sanna, A.; Gross, E. K. U. Bootstrap Approximation for the exchange−correlation Kernel of Time-Dependent Density-Functional Theory. *Phys. Rev. Lett.* **2011**, *107*, No. 186401.
(38) Yang, Z.; Ullrich, C. A. Direct calculation of exciton binding energies with time-dependent density-functional theory. *Phys. Rev. B* **2013**, *87*, No. 195204.
(39) Byun, Y.-M.; Ullrich, C. A. Assessment of long-range-corrected exchange−correlation kernels for solids: Accurate exciton binding energies via an empirically scaled bootstrap kernel. *Phys. Rev. B* **2017**, *95*, No. 205136.
(40) Byun, Y.-M.; Ullrich, C. A. Excitons in solids from time-dependent density-functional theory: Assessing the Tamm- Dancoff approximation. *Computation* **2017**, *5*, 9.
(41) Sun, J.; Yang, J.; Ullrich, C. A. Low-cost alternatives to the Bethe-Salpeter equation: Towards simple hybrid functionals for excitonic effects in solids. *Phys. Rev. Res.* **2020**, *2*, No. 013091.
(42) Sun, J.; Ullrich, C. A. Optical properties of $CsCu_2X_3$ (X = Cl, Br, and I): A comparative study between hybrid time-dependent density-functional theory and the Bethe-Salpeter equation. *Phys. Rev. Mater.* **2020**, *4*, No. 095402.
(43) Bernasconi, L.; Tomić, S.; Ferrero, M.; Rérat, M.; Orlando, R.; Dovesi, R.; Harrison, N. M. First-principles optical response of semiconductors and oxide materials. *Phys. Rev. B* **2011**, *83*, No. 195325.
(44) Bernasconi, L.; Webster, R.; Tomić, S.; Harrison, N. M. Optical response of extended systems from time-dependent Hartree-Fock and time-dependent density-functional theory. *J. Phys.: Conf. Ser.* **2012**, *367*, No. 012001.
(45) Tomić, S.; Bernasconi, L.; Searle, B. G.; Harrison, N. M. Electronic and Optical Structure of Wurtzite $CuInS_2$. *J. Phys. Chem. C* **2014**, *118*, 14478−14484.
(46) Webster, R.; Bernasconi, L.; Harrison, N. M. Optical properties of alkali halide crystals from all-electron hybrid TD-DFT calculations. *J. Chem. Phys.* **2015**, *142*, No. 214705.
(47) Skone, J. H.; Govoni, M.; Galli, G. Self-consistent hybrid functional for condensed systems. *Phys. Rev. B* **2014**, *89*, No. 195112.
(48) Erba, A. Self-consistent hybrid functionals for solids: a fully-automated implementation. *J. Phys.: Condens. Matter* **2017**, *29*, No. 314001.
(49) Linnera, J.; Sansone, G.; Maschio, L.; Karttunen, A. J. Thermoelectric Properties of p-Type Cu_2O, CuO, and NiO from Hybrid Density Functional Theory. *J. Phys. Chem. C* **2018**, *122*, 15180−15189.
(50) Linnera, J.; Karttunen, A. J. Ab initio study of the lattice thermal conductivity of Cu_2O using the generalized gradient approximation and hybrid density functional methods. *Phys. Rev. B* **2017**, *96*, No. 014304.
(51) Becke, A. D. A new mixing of Hartree-Fock and local density-functional theories. *J. Chem. Phys.* **1993**, *98*, 1372−1377.
(52) Lee, C.; Yang, W.; Parr, R. G. Development of the Colle-Salvetti correlation-energy formula into a functional of the electron density. *Phys. Rev. B* **1988**, *37*, 785−789.
(53) Monkhorst, H. J.; Pack, J. D. Special points for Brillouin-zone integrations. *Phys. Rev. B* **1976**, *13*, 5188−5192.
(54) Pinsard-Gaudart, L.; Rodríguez-Carvajal, J.; Gukasov, A.; Monod, P. Magnetic properties of paramelaconite (Cu_4O_3): A pyrochlore lattice with S=1/2. *Phys. Rev. B* **2004**, *69*, No. 104408.
(55) Djurek, D.; Prester, M.; Drobac, D.; Ivanda, M.; Vojta, D. Magnetic properties of nanoscaled paramelaconite Cu_4O_{3-x} (x=0.0 and 0.5). *J. Magn. Magn. Mater.* **2015**, *373*, 183−187.
(56) Pierson, J.; Duverger, E.; Banakh, O. Experimental and theoretical contributions to the determination of optical properties of synthetic paramelaconite. *J. Solid State Chem.* **2007**, *180*, 968−973.

https://dx.doi.org/10.1021/acs.jpcc.0c08270
J. Phys. Chem. C XXXX, XXX, XXX−XXX

(57) Forsyth, J. B.; Brown, P. J.; Wanklyn, B. M. Magnetism in cupric oxide. *J. Phys. C: Solid State Phys.* **1988**, *21*, 2917−2929.
(58) Smart, T. J.; Cardiel, A. C.; Wu, F.; Choi, K.-S.; Ping, Y. Mechanistic insights of enhanced spin polaron conduction in CuO through atomic doping. *npj Comput. Mater.* **2018**, *4*, No. 61.
(59) Živković, A.; de Leeuw, N. H. Exploring the formation of intrinsic p-type and n-type defects in CuO. *Phys. Rev. Mater.* **2020**, *4*, No. 074606.
(60) Runge, E.; Gross, E. K. U. Density-Functional Theory for Time-Dependent Systems. *Phys. Rev. Lett.* **1984**, *52*, 997−1000.
(61) Casida, M. E. Time-dependent density-functional theory for molecules and molecular solids. *J. Mol. Struct.: THEOCHEM* **2009**, *914*, 3−18.
(62) Hirata, S.; Head-Gordon, M. Configuration interaction singles, time- dependent Hartree-Fock, and time- dependent density functional theory for the electronic excited states of extended systems. *J. Chem. Phys.* **1999**, *111*, 10774−10786.
(63) McLachlan, A. D.; Ball, M. A. Time-Dependent Hartree-Fock Theory for Molecules. *Rev. Mod. Phys.* **1964**, *36*, 844−855.
(64) Zangwill, A.; Soven, P. Density-functional approach to local-field effects in finite systems. *Phys. Rev. A* **1980**, *21*, 1561−1572.
(65) Ferrero, M.; Rérat, M.; Orlando, R.; Dovesi, R. Coupled perturbed Hartree-Fock for periodic systems: The role of symmetry and related computational aspects. *J. Chem. Phys.* **2008**, *128*, No. 014110.
(66) Strinati, G. Application of the Green's Functions Method to the Study of the Optical Properties of Semiconductors. In *La Rivista del Nuovo Cimento*; Springer, 1988; Vol. *11*, pp 1−86.
(67) Adamo, C.; Barone, V. Toward reliable density functional methods without adjustable parameters: The PBE0 model. *J. Chem. Phys.* **1999**, *110*, 6158−6170.
(68) Ernzerhof, M.; Scuseria, G. E. Assessment of the Perdew-Burke-Ernzerhof exchange−correlation functional. *J. Chem. Phys.* **1999**, *110*, 5029−5036.
(69) Grondahl, L. O. The Copper-Cuprous-Oxide Rectifier and Photoelectric Cell. *Rev. Mod. Phys.* **1933**, *5*, 141−168.
(70) Lide, D. R. *CRC Handbook of Chemistry and Physics*; CRC Press: Boca Raton, FL, 2005.
(71) Pierson, J. F.; Thobor-Keck, A.; Billard, A. Cuprite, paramelaconite and tenorite films deposited by reactive magnetron sputtering. *Appl. Surf. Sci.* **2003**, *210*, 359−367.
(72) Murali, D. S.; Subrahmanyam, A. Synthesis of low resistive p type Cu_4O_3 thin films by DC reactive magnetron sputtering and conversion of Cu_4O_3 into CuO by laser irradiation. *J. Phys. D.: Appl. Phys.* **2016**, *49*, No. 375102.
(73) Marabelli, F.; Parravicini, G. B. Evidence of localized states in the optical gap of CuO. *Phys. Rev. B: Condens. Matter* **1994**, *199−200*, 255−256.
(74) Ekuma, C.; Anisimov, V.; Moreno, J.; Jarrell, M. Electronic structure and spectra of CuO. *Eur. Phys. J. B* **2014**, *87*, 23.
(75) Reppin, D.; Polity, A.; Meyer, B.; Shokovets, S. Optical and electrical properties of Cu_2O, Cu_4O_3 and CuO. *MRS Online Proc. Libr. Arch.* **2012**, *1494*, 25−31.
(76) Koffyberg, F. P.; Benko, F. A. A photoelectrochemical determination of the position of the conduction and valence band edges of p-type CuO. *J. Appl. Phys.* **1982**, *53*, 1173−1177.
(77) Forsyth, J. B.; Hull, S. The effect of hydrostatic pressure on the ambient temperature structure of CuO. *J. Phys.: Condens. Matter* **1991**, *3*, 5257−5261.
(78) Yang, B. X.; Tranquada, J. M.; Shirane, G. Neutron scattering studies of the magnetic structure of cupric oxide. *Phys. Rev. B* **1988**, *38*, 174−178.
(79) Ray, S. C. Preparation of copper oxide thin film by the sol-gel-like dip technique and study of their structural and optical properties. *Sol. Energy Mater. Sol. Cells* **2001**, *68*, 307−312.
(80) Hu, J. P.; Payne, D. J.; Egdell, R. G.; Glans, P.-A.; Learmonth, T.; Smith, K. E.; Guo, J.; Harrison, N. M. On-site interband excitations in resonant inelastic X-ray scattering from Cu_2O. *Phys. Rev. B* **2008**, *77*, No. 155115.
(81) Heinemann, M.; Eifert, B.; Heiliger, C. Band structure and phase stability of the copper oxides Cu_2O, CuO, and Cu_4O_3. *Phys. Rev. B* **2013**, *87*, No. 115111.
(82) Giar, M.; Heinemann, M.; Heiliger, C. Phonon properties of copper oxide phases from first principles. *Phys. Rev. B* **2017**, *96*, No. 075202.
(83) Rocquefelte, X.; Whangbo, M.-H.; Villesuzanne, A.; Jobic, S.; Tran, F.; Schwarz, K.; Blaha, P. Short-range magnetic order and temperature-dependent properties of cupric oxide. *J. Phys.: Condens. Matter* **2010**, *22*, No. 045502.
(84) Sottile, F.; Karlsson, K.; Reining, L.; Aryasetiawan, F. Macroscopic and microscopic components of exchange−correlation interactions. *Phys. Rev. B* **2003**, *68*, No. 205112.
(85) Sottile, F.; Marsili, M.; Olevano, V.; Reining, L. Efficient ab initio calculations of bound and continuum excitons in the absorption spectra of semiconductors and insulators. *Phys. Rev. B* **2007**, *76*, No. 161103.
(86) Meyer, B. K.; et al. Binary copper oxide semiconductors: From materials towards devices. *Phys. Status Solidi B* **2012**, *249*, 1487−1509.
(87) Ito, T.; Yamaguchi, H.; Okabe, K.; Masumi, T. Single-crystal growth and characterization of Cu_2O and CuO. *J. Mater. Sci.* **1998**, *33*, 3555−3566.

https://dx.doi.org/10.1021/acs.jpcc.0c08270
J. Phys. Chem. C XXXX, XXX, XXX−XXX